

An Exoplanet’s Response to Anisotropic Stellar Mass-Loss During Birth and Death

Dimitri Veras^{1*}, John D. Hadjidemetriou^{2†} and Christopher A. Tout¹

¹*Institute of Astronomy, University of Cambridge, Madingley Road, Cambridge CB3 0HA*

²*Department of Physics, Aristotle University of Thessaloniki, 54124 Thessaloniki, Greece*

Accepted 2013 August 2. Received 2013 July 23; in original form 2013 March 22

ABSTRACT

The birth and death of planets may be affected by mass outflows from their parent stars during the T-Tauri or post-main-sequence phases of stellar evolution. These outflows are often modelled to be isotropic, but this assumption is not realistic for fast rotators, bipolar jets and supernovae. Here we derive the general equations of motion for the time evolution of a single planet, brown dwarf, comet or asteroid perturbed by anisotropic mass loss in terms of a complete set of planetary orbital elements, the ejecta velocity, and the parent star’s co-latitude and longitude. We restrict our application of these equations to 1) rapidly rotating giant stars, and 2) arbitrarily-directed jet outflows. We conclude that the isotropic mass-loss assumption can safely be used to model planetary motion during giant branch phases of stellar evolution within distances of hundreds of au. In fact, latitudinal mass loss variations anisotropically affect planetary motion only if the mass loss is *asymmetric about the stellar equator*. Also, we demonstrate how constant-velocity, asymmetric bipolar outflows in young systems incite orbital inclination changes. Consequently, this phenomenon readily tilts exoplanetary orbits external to a nascent disc on the order of degrees.

Key words: planet-star interactions, planets and satellites: dynamical evolution and stability, stars: evolution, stars: AGB and post-AGB, stars: mass-loss, stars: winds, outflows

1 INTRODUCTION

Planetary evolution and stellar evolution are intertwined. A planet’s birth disc may be periodically ingested by the parent star, triggering episodic mass outbursts that may strongly perturb the planet’s motion. Many Gyr later, during the giant branch phases of the star’s post-main sequence (MS) evolution, the star sheds its mass, also affecting planetary motion. One cannot develop a comprehensive theory for the life cycle of exoplanets without considering such mass-loss events.

Further, there is a strong observational motivation to explore such episodes of mass loss. Mounting discoveries of planets orbiting post-MS stars are becoming too numerous to list individually in one paper; see Table 6 of Gettel et al. (2012) for a reliable recent summary. Explanations for their currently observed orbital parameters, as well as their past history and eventual fate, require accurate models of stellar mass loss in conjunction with orbital motion and potentially other effects such as tides. No planets have so far been confirmed orbiting white dwarfs. This finding, as pointed out by Mustill & Villaver (2012), exemplifies the need to understand orbital evolution around giant

stars so that future campaigns to search for planets around white dwarfs are motivated and well-directed.

The dearth of analyses of exoplanetary motion owing to mass loss has been partially alleviated in the last decade, primarily with post-MS studies. Although the general two-body problem with mass loss has a long history (see Rahoma et al. 2009 for a review), only recently have these analyses been directed towards understanding exoplanetary systems. Of particular interest to exoplanetary scientists is the time evolution of orbital elements such as semimajor axis (a), eccentricity (e), inclination (i), longitude of ascending node (Ω) and argument of pericentre (ω). This preference is partly reflected in the parameters which are reported in the major exoplanet databases (the Extrasolar Planets Encyclopedia at <http://exoplanet.eu/>, the Exoplanet Data Explorer at <http://exoplanets.org/> and the NASA Exoplanet Archive at <http://exoplanetarchive.ipac.caltech.edu/>). The earliest studies which presented expressions for this time evolution (Omarov 1962; Hadjidemetriou 1963) helped lay the groundwork for future research conducted after the first hints of later-confirmed exoplanets (Campbell et al. 1988; Latham et al. 1989) and the first confirmed exoplanets (Wolszczan & Frail 1992). This research specifically includes effects which may cause an exoplanet to escape from a post-MS system (Veras et al. 2011; Veras & Tout 2012; Adams et al. 2013) and generally encom-

* E-mail: veras@ast.cam.ac.uk

† Please see Acknowledgements

passes studies investigating a planet engulfed by its expanding star (Villaver & Livio 2007, 2009; Nordhaus et al. 2010; Villaver 2011; Mustill & Villaver 2012; Passy et al. 2012; Spiegel 2012; Nordhaus & Spiegel 2013) as well as massive planet scattering in post-MS systems (Debes & Sigurdsson 2002; Bonsor et al. 2011, 2012; Debes et al. 2012; Veras et al. 2013; Voyatzis et al. 2013).

However, in every one of these cases, mass loss is assumed to be isotropic. Anisotropic mass-loss studies considering planetary motion are rare, and require care with respect to the reference frame used. These studies include those by Boué et al. (2012) and Iorio (2012), both of whom consider anisotropic evaporation from planetary atmospheres as the driver for orbital evolution. Investigators who instead consider asymmetric mass loss from the central star include Parriott & Alcock (1998), who quantify the escape of comets in different directions during post-MS evolution, and Namouni (2005), Namouni & Zhou (2006), Namouni & Guzzo (2007), and Namouni (2013), who instead look at the effects of bipolar jets on planetary orbits during the early stages of the life of a planetary system.

These early stages are also important to consider because the vast majority of known exoplanets are observed during MS evolution. Therefore, their measured orbital parameters may have been strongly influenced by the parent star's behaviour while the protoplanetary birth disc was still present. Systems with violent nebular histories featuring mass loss may be the source of some exoplanet eccentricities (Namouni 2005). We will show how planetary inclinations may be similarly excited. Although the vast majority of exoplanet inclinations are unknown, hints from highly inclined hot Jupiters (e.g. Winn et al. 2009; Addison et al. 2013; Zhou & Huang 2013) as well as the Solar System illustrate that planets do not necessarily always form on planar orbits.

Here, we derive the complete equations of motion for the time evolution of planetary orbital elements accounting for latitude-, longitude- and time-dependent stellar mass loss. Subsequently, by invoking symmetries in stellar mass loss models, we place strong constraints on the resulting orbital motion. Although these equations have several applications, we choose two for this study. The first is simply to quantify the goodness of the isotropic mass-loss approximation for planetary evolution in post-MS systems. The second is to show how simply-approximated bipolar jets which are formed in the nascent stages of a planetary system can excite orbital inclinations. We derive the equations of motion in Section 2 and apply them in Section 3 to post-MS evolution (Section 3.1) and pre-MS evolution (Section 3.2) before concluding in Section 4.

2 EQUATIONS OF MOTION

Our goal in this section is to express the time evolution of the orbital elements $(a, e, i, \Omega, \omega)$ in terms of one another and as a function of position- and velocity-dependent mass ejection. We begin by considering the equations of motion in Cartesian coordinates.

2.1 Inertial Frame

Suppose a planet of constant mass M_p is orbiting a solid body star of mass $M_s(t)$, so that the total system mass is $M(t) = M_s(t) + M_p$. The stellar mass-loss flux, denoted by $J(\phi, \theta, t) > 0$,

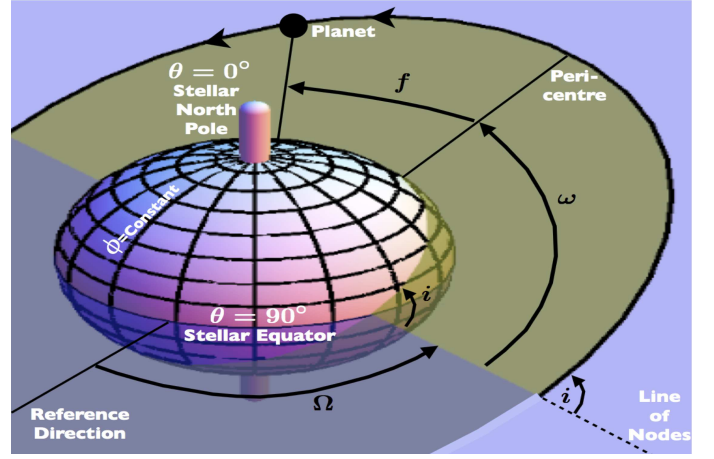


Figure 1. Illustration displaying stellar co-latitude (θ), stellar longitude (ϕ), inclination (i), longitude of ascending node (Ω), argument of pericentre (ω) and true anomaly (f).

is the mass-loss rate per steradian. Here, ϕ is the stellar longitude and θ is the stellar co-latitude. Therefore,

$$\frac{dM(t)}{dt} = \frac{dM_s(t)}{dt} = -\frac{1}{4\pi} \int_0^\pi \int_0^{2\pi} J(\phi, \theta, t) \sin \theta d\phi d\theta. \quad (1)$$

The mass is lost at velocity $\vec{u}(\phi, \theta, t)$, where \vec{u} is a vector along the radius of the star. Under the simplifying assumption that the direction of the rotational axis of the star is fixed with respect to the orbit of the planet, then the equations of motion of the system are

$$M_p \ddot{\vec{R}}_p = \frac{GM_p M_s(t)}{|\vec{R}_s - \vec{R}_p|^3} (\vec{R}_s - \vec{R}_p), \quad (2)$$

$$M_s(t) \ddot{\vec{R}}_s = \frac{GM_s(t) M_p}{|\vec{R}_p - \vec{R}_s|^3} (\vec{R}_p - \vec{R}_s) + \vec{F}, \quad (3)$$

such that $\vec{F} = \mathbf{Q}\vec{P}$, where

$$\vec{P} = \begin{pmatrix} \frac{1}{4\pi} \int_0^\pi \int_0^{2\pi} J(\phi, \theta, t) u(\phi, \theta, t) \cos \phi \sin \theta d\phi d\theta \\ \frac{1}{4\pi} \int_0^\pi \int_0^{2\pi} J(\phi, \theta, t) u(\phi, \theta, t) \sin \phi \sin \theta d\phi d\theta \\ \frac{1}{4\pi} \int_0^\pi \int_0^{2\pi} J(\phi, \theta, t) u(\phi, \theta, t) \cos \theta d\phi d\theta \end{pmatrix} \quad (4)$$

and the matrix \mathbf{Q} transforms from the spin from the star to the orbital plane and has components

$$Q_{11} = \cos \Omega \cos \omega - \sin \Omega \sin \omega \cos i, \quad (5)$$

$$Q_{21} = \sin \Omega \cos \omega + \cos \Omega \sin \omega \cos i, \quad (6)$$

$$Q_{31} = \sin \omega \sin i, \quad (7)$$

$$Q_{12} = -\cos \Omega \sin \omega - \sin \Omega \cos \omega \cos i, \quad (8)$$

$$Q_{22} = -\sin \Omega \sin \omega + \cos \Omega \cos \omega \cos i, \quad (9)$$

$$Q_{32} = \cos \omega \sin i, \quad (10)$$

$$Q_{13} = \sin \Omega \sin i, \quad (11)$$

$$Q_{23} = -\cos \Omega \sin i, \quad (12)$$

$$Q_{33} = \cos i. \quad (13)$$

The angles θ , ϕ , i , Ω and ω are illustrated in Fig. 1, along with the true anomaly f .

2.2 Rotational Frame

The equations of the relative motion can be obtained if we subtract equation (3) from equation (2). Defining the relative position of the planet with respect to the star by \vec{r} , where

$$\vec{r} = \vec{R}_p - \vec{R}_s, \quad (14)$$

we have

$$\ddot{\vec{r}} = -\frac{GM(t)}{r^3}\vec{r} - \frac{\vec{F}}{M_s(t)}. \quad (15)$$

As a check, we can consider the isotropic mass-loss case. For isotropic mass-loss, J and \vec{u} are constant for all ϕ and θ and are unchanging in time. Then, $\vec{P} = 0$ and hence $\vec{F} = 0$. This result is expected because, in the isotropic case, the perturbation to the motion due to mass-loss is implicit in $M_s(t)$. Omarov (1962), Hadjidemetriou (1963) and Deprit (1983) found that this implicit perturbation to equal

$$\vec{D} = -\frac{1}{2}\frac{\dot{M}(t)}{M(t)}\vec{r}, \quad (16)$$

which can be used to derive the equations of motion for the planet in orbital elements in the isotropic case (e.g. Veras et al. 2011).

2.3 Orbital Parameter Evolution

Now, we wish to express the equations of motion in terms of the time evolution of planetary orbital elements. To do so, we use the generalized perturbation equations of Veras & Evans (2013). The total perturbation to the two-body problem is then composed of both an implicit and explicit term, as in equations (15)-(16), and is equal to

$$\vec{D} - \frac{\vec{F}}{M_s}. \quad (17)$$

We can apply each of these terms separately to the perturbation equations, and then add the result. When doing so, we note importantly that although \vec{F} is a function of \vec{u} , \vec{F} is not a function of the planet's position nor its velocity. We obtain

$$\frac{da}{dt} = \left(\frac{da}{dt}\right)_{\text{iso}} + \left(\frac{da}{dt}\right)_{\text{aniso}}, \quad (18)$$

$$\frac{de}{dt} = \left(\frac{de}{dt}\right)_{\text{iso}} + \left(\frac{de}{dt}\right)_{\text{aniso}}, \quad (19)$$

$$\frac{di}{dt} = \left(\frac{di}{dt}\right)_{\text{iso}} + \left(\frac{di}{dt}\right)_{\text{aniso}}, \quad (20)$$

$$\frac{d\Omega}{dt} = \left(\frac{d\Omega}{dt}\right)_{\text{iso}} + \left(\frac{d\Omega}{dt}\right)_{\text{aniso}}, \quad (21)$$

$$\frac{d\omega}{dt} = \left(\frac{d\omega}{dt}\right)_{\text{iso}} + \left(\frac{d\omega}{dt}\right)_{\text{aniso}}, \quad (22)$$

$$\begin{aligned} \frac{df}{dt} &= \left(\frac{df}{dt}\right)_{\text{unperturbed 2-body}} + \left(\frac{df}{dt}\right)_{\text{mass loss}} \\ &= \frac{n(1+e\cos f)^2}{(1-e^2)^{3/2}} - \frac{d\omega}{dt} - \cos i \frac{d\Omega}{dt}, \end{aligned} \quad (23)$$

where n refers to the planet's mean motion. The unperturbed 2-body term is the only term from equations (18)-(23) which survives when $J = 0$.

2.3.1 General Equations

By using the procedure of Veras & Evans (2013) with the perturbation given by equation (17), we obtain the complete equations of motion for the planet. The isotropic contributions are

$$\left(\frac{da}{dt}\right)_{\text{iso}} = -\frac{a(1+e^2+2e\cos f)}{1-e^2} \frac{1}{M} \frac{dM}{dt}, \quad (24)$$

$$\left(\frac{de}{dt}\right)_{\text{iso}} = -(e+\cos f) \frac{1}{M} \frac{dM}{dt}, \quad (25)$$

$$\left(\frac{di}{dt}\right)_{\text{iso}} = 0, \quad (26)$$

$$\left(\frac{d\Omega}{dt}\right)_{\text{iso}} = 0, \quad (27)$$

$$\left(\frac{d\omega}{dt}\right)_{\text{iso}} = -\frac{\sin f}{e} \frac{1}{M} \frac{dM}{dt}, \quad (28)$$

(29)

which represents the standard set from Omarov (1962), Hadjidemetriou (1963) and Veras et al. (2011). These are the only surviving terms when $\vec{F} = 0$. The non-isotropic terms are

$$\begin{aligned} \left(\frac{da}{dt}\right)_{\text{aniso}} &= -\frac{2}{nM_s\sqrt{1-e^2}} \left[\right. \\ &\quad -\left\{C_1 \cos i \sin \Omega + C_2 \cos \Omega\right\}F_x \\ &\quad \left. + \left\{C_1 \cos i \cos \Omega - C_2 \sin \Omega\right\}F_y + \left\{C_1 \sin i\right\}F_z \right], \end{aligned} \quad (30)$$

$$\begin{aligned} \left(\frac{de}{dt}\right)_{\text{aniso}} &= -\frac{\sqrt{1-e^2}}{2anM_s(1+e\cos f)} \left[\right. \\ &\quad -\left\{C_6 \cos i \sin \Omega + C_5 \cos \Omega\right\}F_x \\ &\quad \left. + \left\{C_6 \cos i \cos \Omega - C_5 \sin \Omega\right\}F_y + \left\{C_6 \sin i\right\}F_z \right], \end{aligned} \quad (31)$$

$$\begin{aligned} \left(\frac{di}{dt}\right)_{\text{aniso}} &= -\frac{\sqrt{1-e^2}}{anM_s(1+e\cos f)} \left[\right. \\ &\quad +\left\{\sin i \sin \Omega \cos(f+\omega)\right\}F_x \\ &\quad -\left\{\sin i \cos \Omega \cos(f+\omega)\right\}F_y \\ &\quad \left. + \left\{\cos i \cos(f+\omega)\right\}F_z \right], \end{aligned} \quad (32)$$

$$\begin{aligned} \left(\frac{d\Omega}{dt}\right)_{\text{aniso}} &= -\frac{\sqrt{1-e^2} \sin(f+\omega)}{anM_s(1+e\cos f)} \left[\right. \\ &\quad +\left\{\sin \Omega\right\}F_x - \left\{\cos \Omega\right\}F_y + \left\{\cot i\right\}F_z \left. \right], \end{aligned} \quad (33)$$

$$\begin{aligned} \left(\frac{d\omega}{dt}\right)_{\text{aniso}} &= -\frac{\sqrt{1-e^2}}{2aenM_s(1+e\cos f)} \left[\right. \\ &\quad -\left\{-C_8 \cos i \sin \Omega + C_7 \cos \Omega\right\}F_x \end{aligned}$$

$$\begin{aligned}
& -\left\{C_8 \cos i \cos \Omega + C_7 \sin \Omega\right\} F_y \\
& -\left\{C_8 \sin i + e \sin (f + \omega) \left[\tan \frac{i}{2} + \cot \frac{i}{2}\right]\right\} F_z, \quad (34)
\end{aligned}$$

where the auxiliary set of C_i variables are:

$$\begin{aligned}
C_1 & \equiv e \cos \omega + \cos (f + \omega), \\
C_2 & \equiv e \sin \omega + \sin (f + \omega), \\
C_5 & \equiv (3 + 4e \cos f + \cos 2f) \sin \omega + 2(e + \cos f) \cos \omega \sin f, \\
C_6 & \equiv (3 + 4e \cos f + \cos 2f) \cos \omega - 2(e + \cos f) \sin \omega \sin f, \\
C_7 & \equiv (3 + 2e \cos f - \cos 2f) \cos \omega + \sin \omega \sin 2f, \\
C_8 & \equiv (3 - \cos 2f) \sin \omega - 2(e + \cos f) \cos \omega \sin f.
\end{aligned}$$

We wish to express equations (30)–(34) in terms of properties of anisotropic stellar mass loss. These are manifested in \vec{P} . Inserting $\vec{F} = \mathbf{Q}\vec{P}$ into these equations yields remarkable simplifications

$$\left(\frac{da}{dt}\right)_{\text{aniso}} = \frac{2}{nM_s \sqrt{1-e^2}} \left[(\sin f) P_x - (e + \cos f) P_y \right], \quad (35)$$

$$\begin{aligned}
\left(\frac{de}{dt}\right)_{\text{aniso}} &= \frac{\sqrt{1-e^2}}{2anM_s (1+e \cos f)} \left[\right. \\
& \left. + 2 \sin f (e + \cos f) P_x - (3 + 4e \cos f + \cos 2f) P_y \right], \quad (36)
\end{aligned}$$

$$\left(\frac{di}{dt}\right)_{\text{aniso}} = -\frac{\sqrt{1-e^2} \cos (f + \omega)}{anM_s (1+e \cos f)} P_z, \quad (37)$$

$$\left(\frac{d\Omega}{dt}\right)_{\text{aniso}} = -\frac{\sqrt{1-e^2} \sin (f + \omega) \csc i}{anM_s (1+e \cos f)} P_z, \quad (38)$$

$$\begin{aligned}
\left(\frac{d\omega}{dt}\right)_{\text{aniso}} &= \frac{\sqrt{1-e^2}}{2aenM_s (1+e \cos f)} \left[-(\sin 2f) P_y \right. \\
& \left. + (3 + 2e \cos f - \cos 2f) P_x + 2 \cot i \sin (f + \omega) P_z \right]. \quad (39)
\end{aligned}$$

Equations (35)–(39) are one of the main results of this study. They show explicitly how the time evolution of the orbital parameters relates to stellar mass loss at a given latitude and longitude. Although we have not found these relations in existing literature, we can use previous studies to help corroborate parts of our equations. The most direct link is with Omarov (1962). The coefficients of the three P_z terms in our equations (37)–(39) are exactly equal to the coefficients of the f_3 terms in equation (13) of Omarov (1962) or equations (21)–(23) of the similar, English-language work by Omarov (1964)¹. Similarly, although Iorio (2012) treats anisotropic mass loss from the planet instead of the star and uses Gauss' planetary equations, which are derived with small perturbations, his coefficients for di/dt and $d\Omega/dt$ in his equation (18) are equivalent to those in our equations (37)–(38). Boué et al. (2012) also assume anisotropic mass loss from the planet, apply a specific form for mass loss

¹ The coefficients of the other components cannot be compared because of the different choices of fiducial velocities chosen in equation (8) of Omarov (1962) and equation (5) of Veras & Evans (2013).

and do not utilize the true anomaly. Nevertheless, the dependencies in their equation (7) can be compared to those in our equations (35)–(36).

One can deduce several interesting properties from our general equations of motion.

- 1) The non-isotropic terms become increasingly important the further away the planet resides from the star because these terms contain an additional factor of \sqrt{a} .
- 2) For a fixed total system mass, if the secondary is a brown dwarf or other type of star instead of a planet, the effects of anisotropic mass loss are diminished. Similarly the importance of the anisotropic terms is maximized for test particle secondaries.
- 3) The evolution of the semimajor axis, eccentricity and longitude of pericentre remain independent of i and Ω , as in the isotropic case.
- 4) A planet with an initially circular orbit does not retain that orbit. Similarly, a planet's orbital inclination with respect to the stellar rotation axis is always changing.

2.3.2 Adiabatic Equations

For many cases of interest, the planet's orbital period is much smaller than the mass-loss timescale². This comparison remains true for a planet within a few hundred au of any star that becomes a white dwarf (Veras et al. 2011). In these cases, we can average over the true anomaly in equations (35)–(39)³. We do so in the same manner as Veras & Evans (2013), where for an arbitrary variable β ,

$$\frac{d\beta}{dt}_{\text{adiabatic}} = \frac{n}{2\pi} \int_0^{2\pi} \frac{d\beta}{dt}_{\text{non-adiabatic}} \frac{dt}{df} df, \quad (40)$$

and we assume

$$\frac{dt}{df} = \frac{(1-e^2)^{3/2}}{n(1+e \cos f)^2}. \quad (41)$$

The quality of this approximation for the isotropic case is computed in equations (17–20) of Veras et al. (2011) and illustrated in fig. 1 of that paper. They show that the adiabatic eccentricity variation from the initial value has an amplitude which is of the same order of the mass loss rate. Averaging over the isotropic terms here yields

$$\left(\frac{da}{dt}\right)_{\text{iso}}^{\text{adi}} = -\frac{a}{M} \frac{dM}{dt}, \quad (42)$$

$$\left(\frac{de}{dt}\right)_{\text{iso}}^{\text{adi}} = \left(\frac{di}{dt}\right)_{\text{iso}}^{\text{adi}} = \left(\frac{d\Omega}{dt}\right)_{\text{iso}}^{\text{adi}} = \left(\frac{d\omega}{dt}\right)_{\text{iso}}^{\text{adi}} = 0. \quad (43)$$

Conversely, averaging over the non-isotropic terms causes only the da/dt term to vanish so that

$$\left(\frac{da}{dt}\right)_{\text{aniso}}^{\text{adi}} = 0, \quad (44)$$

² In this approximation, the planetary orbit behaves adiabatically in the sense that its eccentricity is conserved; see Debes & Sigurdsson (2002) and Veras et al. (2011).

³ One should not average over equations (30)–(34) first and then insert $\vec{F} = \mathbf{Q}\vec{P}$ into the resulting equations. Doing so yields unphysical dependencies on \vec{P} .

$$\left(\frac{de}{dt}\right)_{\text{aniso}}^{\text{adi}} = -\frac{3\sqrt{1-e^2}}{2anM_s}P_y, \quad (45)$$

$$\left(\frac{di}{dt}\right)_{\text{aniso}}^{\text{adi}} = \frac{3e \cos \omega}{2anM_s\sqrt{1-e^2}}P_z, \quad (46)$$

$$\left(\frac{d\Omega}{dt}\right)_{\text{aniso}}^{\text{adi}} = -\frac{3e \sin \omega \csc i}{2anM_s\sqrt{1-e^2}}P_z, \quad (47)$$

$$\left(\frac{d\omega}{dt}\right)_{\text{aniso}}^{\text{adi}} = \frac{3}{2aenM_s} \times \left(\sqrt{1-e^2}P_x - \frac{e^2}{\sqrt{1-e^2}}\sin \omega \cot i P_z\right). \quad (48)$$

Equations (44)–(48) are another main result of this paper and allow us to deduce planetary orbital properties directly from the character of anisotropic stellar mass loss in \vec{P} for most planets within a few hundred au of their parent star. For planets or comets which are further away, we must use equations (23) and (35)–(39). Properties of the adiabatic equations include the following.

- 1) Instability may occur, unlike the adiabatic isotropic case. Regardless of the planet's semimajor axis, its eccentricity may approach unity and hence collide with the star.
- 2) Anisotropic terms are retained after averaging in each equation except for da/dt , and the time evolution of e , I , Ω and ω are each proportional to \sqrt{a} .
- 3) Unlike the isotropic case, initially circular or coplanar orbits are not guaranteed to remain so.

3 APPLICATIONS

Here we present examples of how the above equations might be applied to studies focused on a particular exosystem.

3.1 Post-MS Rotation

We first consider planetary dynamical evolution in post-MS systems, where stellar rotation is linked to mass loss. We discuss the dependence on co-latitude and then longitude before moving on to specific examples.

3.1.1 Latitudinal Dependence

Several authors have investigated physically sensible scaling laws for mass loss and velocity ejecta as a function of θ . In a seminal paper describing stellar winds, Castor et al. (1975) establish a scaling law for mass loss (their equation 46) in terms of intrinsic stellar properties. Owocki et al. (1998) re-expressed this law in a form more useful for our purposes,

$$J = J(\theta = 0, t) \left[\frac{H(\theta)}{H(\theta = 0)}\right]^{\frac{1}{\alpha}} \left[1 - \frac{V_{\text{rot}}^2 p_s}{GM_s(t)} \sin^2 \theta\right]^{1-\frac{1}{\alpha}}, \quad (49)$$

where p_s is the radius of the star, V_{rot} is the rotational velocity of the star at the equator, H is the radiative flux and α is an empirically-determined constant. Puls et al. (2008) provide recent estimates of $0.6 \lesssim \alpha \lesssim 0.7$ for O-type stars and $\alpha \approx 0.45$ for A supergiants. These estimates broadly agree with more recent adoptions of $\alpha \approx 0.60$ (Lovekin 2011) and $\alpha = 0.43$ (Georgy et al. 2011). However, we can simplify the expression

for $J(\phi, \theta, t)$ and thereby eliminate the dependence on α by considering the gravity darkening law of von Zeipel (1924) so that

$$\frac{H(\theta)}{H(\theta = 0)} = 1 - \frac{V_{\text{rot}}^2 p_s}{GM_s(t)} \sin^2 \theta. \quad (50)$$

Owocki et al. (1998) also provide an estimate for latitudinally-varying ejecta speed

$$u(\phi, \theta, t) = \sqrt{\left(\frac{2GM_s(t)}{p_s}\right) \left(1 - \frac{V_{\text{rot}}^2 p_s}{GM_s(t)} \sin^2 \theta\right)}. \quad (51)$$

Equations (49)–(51) have no longitudinal dependence. Consequently, the double integrals in the expression for \vec{F} become

$$P_x = \frac{1}{4\pi} \int_0^{2\pi} \cos \phi d\phi \int_0^\pi J(\theta, t) u(\theta, t) \sin \theta d\theta = 0, \quad (52)$$

$$P_y = \frac{1}{4\pi} \int_0^{2\pi} \sin \phi d\phi \int_0^\pi J(\theta, t) u(\theta, t) \sin \theta d\theta = 0, \quad (53)$$

$$P_z = \frac{1}{4\pi} \int_0^{2\pi} d\phi \int_0^\pi J(\theta, t) u(\theta, t) \cos \theta d\theta = \frac{1}{2} J(\theta = 0, t) \times \sqrt{\frac{2GM_s(t)}{p_s}} \int_0^\pi \left[1 - \frac{V_{\text{rot}}^2 p_s}{GM_s(t)} \sin^2 \theta\right]^{\frac{3}{2}} \cos \theta d\theta = 0. \quad (54)$$

The last integral shows that despite the latitudinal dependencies, mass loss which is symmetric about the stellar equator has no net effect on a planet's motion in addition to the usual effect from isotropic mass loss. This result helps verify the robustness of the isotropic mass loss approximation in post-MS studies.

Nevertheless, let us consider the possibility that mass-loss is not symmetric about the equator. Here we assume that the mass loss from the northern hemisphere of the star is $k > 1$ times the amount of mass lost from the southern hemisphere and adopt the same latitudinal dependence as in equation (49) and velocity dependence as in equation (51). Also, let us describe the square of the ratio of the rotational velocity to the circular velocity at the stellar surface by $T(t) \equiv V_{\text{rot}}^2 p_s / (GM_s(t))$. Also, let $J_0(t) \equiv J(\theta = 0, t)$. Then,

$$P_z = J_0(t) (k - 1) V_{\text{rot}} \times \frac{(2T(t) - 5) \sqrt{2T(t)(1 - T(t))} + 3\sqrt{2} \arcsin \sqrt{T(t)}}{16T(t)}, \quad (55)$$

or, in the small $T(t)$ approximation,

$$P_z \approx J_0(t) (k - 1) V_{\text{rot}} \left(-\frac{1}{4\sqrt{2T(t)}} + \frac{5\sqrt{T(t)}}{8\sqrt{2}}\right), \quad (56)$$

while still $P_x = P_y = 0$. Consequently, in the adiabatic approximation, the eccentricity remains static.

3.1.2 Longitudinal Dependence

Here we explore the case of variation in mass loss with longitude. Let us assume the velocity dependence in equation (51) holds, and the dependence of J on θ and ϕ are decoupled, so that $J = J_0 j(\phi) j(\theta)$. Here, $j(\theta) = 1 - T(t) \sin^2 \theta$, as in equation (49). Then,

$$P_x = \left[5 - 3T(t) + \frac{3(T(t) - 1)^2 \operatorname{arctanh} \sqrt{T(t)}}{\sqrt{T(t)}}\right]$$

$$\times \frac{1}{8} J_0(t) V_{\text{rot}} \sqrt{\frac{2}{T(t)}} \int_0^{2\pi} j(\phi) \cos \phi d\phi, \quad (57)$$

or, in the small $T(t)$ approximation,

$$P_x \approx J_0(t) V_{\text{rot}} \left(\sqrt{\frac{2}{T(t)}} - \sqrt{2T(t)} \right) \int_0^{2\pi} j(\phi) \cos \phi d\phi, \quad (58)$$

and similarly for P_y except with $\cos \phi$ replaced with $\sin \phi$. Also, $P_z = 0$. Consequently, in both the general equations of motion and the adiabatic approximation, a planet's inclination and longitude of ascending node do not change owing to these longitudinal perturbations.

By analogy with the latitudinal case, let us consider when the mass lost from the eastern hemisphere of the star is $k > 1$ times the amount of mass lost from the western hemisphere. We assume the eastern hemisphere is defined by the region bounded by $\phi = 0$ and $\phi = \pi$. Then $P_x = 0$ and

$$P_y = \frac{k-1}{4} J_0(t) V_{\text{rot}} \sqrt{\frac{2}{T(t)}} \times \left[5 - 3T(t) + \frac{3(T(t)-1)^2 \operatorname{arctanh} \sqrt{T(t)}}{\sqrt{T(t)}} \right], \quad (59)$$

or, in the small $T(t)$ approximation,

$$P_y \approx J_0(t) V_{\text{rot}} (k-1) \left(\sqrt{\frac{8}{T(t)}} - \sqrt{8T(t)} \right). \quad (60)$$

Although this perturbation causes changes in the planetary eccentricity, the argument of pericentre remains static.

3.1.3 Specific Examples

We have shown (equations 52–54) that the isotropic mass loss assumption is an excellent, physically-motivated approximation to use for planetary motion in post-MS systems. Now let us consider the possibility that the stars do not behave according to equations (49)–(51). Then, generally, $\vec{P} \neq 0$ and we may obtain relations such as equations (55)–(56) or equations (59)–(60). The question we wish to answer is, “How extremely asymmetric must giant star mass-loss be in order for the anisotropy to make a meaningful change in planetary orbit evolution?” In order to conduct numerical simulations, we must first obtain physically-motivated values for M_s , p_s , J_0 and V_{rot} .

We choose the mass of the star to be below that at which it would end its life in a supernova so $M_s \lesssim 8M_\odot$ for Solar metallicity and $M_s \lesssim 6M_\odot$ at $Z = 10^{-4}$ (Hurley et al. 2000). Known exoplanet host stars nearly always have masses which are less than $3M_\odot$, although this mass barrier has recently been broken (Sato et al. 2012) and a few brown dwarfs might orbit significantly more massive stars (e.g. Hatzes et al. 2005).

The equatorial radius p_s of the star is important because it expands dramatically during the post-MS. Often p_s reaches a distance in au that is approximately equal to the number of solar masses in the star's progenitor mass (see e.g. Fig. 2 of Veras et al. 2013). Consequently, a planet may be engulfed by the expanding envelope. Even if a planet escapes this fate, the planet may be affected by tidal forces from the envelope. The expansion also affects the spin of the star, because conservation of angular momentum dictates that stellar expansion in inversely

correlated with a star's rotational velocity. We discuss this point further in Section 3.1.4.

The other parameters, J_0 and V_{rot} , are poorly constrained observationally. Additionally, much of the focus on stellar rotation theory centres around supernova progenitor stars with $M_s \gtrsim 8M_\odot$ (e.g. Heger et al. 2000; Ekström et al. 2008; Lovekin 2011), which are not our focus here. Further, the time evolution of the rotational velocity of a post-MS star may be a strong function of the character of the mass loss (see, e.g., fig. 4 of Maeder 2002). To help constrain our search for realistic values of J_0 and V_{rot} , we consider two phases of post-MS evolution, the RGB and AGB phases.

Consider first J_0 . For white dwarf progenitors with masses greater than about $2M_\odot$, the greatest combined mass loss occurs on the AGB (see e.g. fig. 7 of Veras et al. 2013), and in particular at the tip of the AGB (e.g. Vassiliadis & Wood 1993). Except for the AGB most mass loss typically occurs on the RGB. The maximum mass-loss rate, however, nearly always occurs on the AGB, even accounting for the six different formulations of mass loss in RGB stars considered by Catelan (2009) [Reimers, Modified Reimers, Mullan, Goldberg, Judge-Stencel, and VandenBerg]. Empirical fits to observations (e.g. Hurley et al. 2000) demonstrate that, in some cases, stars with $M_s(t=0) \approx 8M_\odot$ can maintain mass-loss rates of the order of $10^{-4} M_\odot \text{yr}^{-1}$ for the order of 10^4 yr. These numbers may change to $10^{-6} M_\odot \text{yr}^{-1}$ and 10^4 yr for some $1M_\odot$ stars, and $10^{-8} M_\odot \text{yr}^{-1}$ and 10^7 yr for other $1M_\odot$ stars (see e.g. Veras & Wyatt 2012). During the period of greatest mass loss, at the tip of the AGB, p_s is near its maximum value.

Now consider V_{rot} . The rotational velocities of stars are bounded from below by zero and from above by that equatorial velocity at which a star would break up. This critical velocity is generally a function of the stellar luminosity. Maeder & Meynet (2000) investigate expressions for the critical velocity in detail; we are interested in the maximum of these values, so that we can have a representative range of potential rotation velocities to apply to our formulae. They show $v_{\text{crit,max}} = \sqrt{2GM_s/(3p_{\text{polar}})}$, where $p_{\text{polar}} = 2p_s/3$. Hence, at the maximum critical velocity $T = 1$, and the equations (55) and (59) become

$$P_z(T=1) = \frac{3\sqrt{2}\pi}{32} (k-1) J_0 V_{\text{rot}} \approx 0.4 (k-1) J_0 V_{\text{rot}}, \quad (61)$$

and

$$P_y(T=1) = \frac{\sqrt{2}}{2} (k-1) J_0 V_{\text{rot}} \approx 0.7 (k-1) J_0 V_{\text{rot}}. \quad (62)$$

For stars which do not rotate at all, $T = 0$, and

$$\begin{aligned} P_z(T=0) &= -\frac{(k-1)}{4\sqrt{2}} J_0 \sqrt{\frac{GM_s}{p_s}} \\ &\approx -0.2 (k-1) J_0 \sqrt{\frac{GM_s}{p_s}}, \end{aligned} \quad (63)$$

$$\begin{aligned} P_y(T=0) &= 2\sqrt{2} (k-1) J_0 \sqrt{\frac{GM_s}{p_s}} \\ &\approx 2.8 (k-1) J_0 \sqrt{\frac{GM_s}{p_s}}. \end{aligned} \quad (64)$$

All these considerations lead us to choose the parameters presented in Table 1. Although this work is not meant to represent an exhaustive phase space study, we have sampled a representative range of each parameter in the table. In the first

Table 1. Model parameters for Figs. 2–3. The variable t_f refers to the duration of the mass loss, M_p the mass of the planet or other stellar companion, $M_s(0)$ the progenitor mass of the parent star, $M_s(t_f)$ the mass of the parent star at time t_f , p_s the parent star's radius, V_{rot} the rotational velocity of the star at the equator, $u(\theta)$ the mass outflow velocity distribution, $u(\theta = 0^\circ)$ the polar mass outflow velocity, $a(0)$ the initial semimajor axis, $e(0)$ the initial eccentricity, and $f(0)$ the initial true anomaly.

Model #	$\frac{t_f}{\text{Myr}}$	$\frac{M_p}{M_\odot}$	$\frac{M_s(0)}{M_\odot}$	$\frac{M_s(t_f)}{M_s(0)}$	$\frac{p_s}{\text{au}}$	$\frac{V_{\text{rot}}}{\text{km/s}}$	$\frac{V_{\text{rot}}}{v_{\text{crit,max}}}$	$u(\theta)$	$\frac{u(\theta=0^\circ)}{\text{km/s}}$	$\frac{a(0)}{\text{au}}$	$e(0)$	$f(0)$
Adiabatic with Total Initial Mass = $1M_\odot$												
1.1	1.0	0	1.000	0.80	1.0	–	–	flat	50.0	35.0	0.25	–
1.2	1.0	0	1.000	0.70	1.0	–	–	flat	50.0	35.0	0.25	–
1.3	1.0	0	1.000	0.60	1.0	–	–	flat	50.0	35.0	0.25	–
1.4	1.0	0	1.000	0.50	1.0	–	–	flat	50.0	35.0	0.25	–
1.5	10.0	0	1.000	0.80	1.0	–	–	flat	50.0	35.0	0.25	–
1.6	10.0	0	1.000	0.70	1.0	–	–	flat	50.0	35.0	0.25	–
1.7	10.0	0	1.000	0.60	1.0	–	–	flat	50.0	35.0	0.25	–
1.8	10.0	0	1.000	0.50	1.0	–	–	flat	50.0	35.0	0.25	–
1.9	100.0	0	1.000	0.50	1.0	–	–	flat	50.0	35.0	0.25	–
Adiabatic with Total Initial Mass = $2M_\odot$ and Total Final Mass = $0.8M_\odot$												
2.1	1.500	0.001	1.999	0.40	2.0	–	–	flat	0.1	4.00	0.1	–
2.2	1.500	0.001	1.999	0.40	2.0	–	–	flat	1.0	4.00	0.1	–
2.3	1.500	0.001	1.999	0.40	2.0	–	–	flat	10.0	4.00	0.1	–
2.4	1.500	0.001	1.999	0.40	2.0	–	–	flat	100.0	4.00	0.1	–
2.5	1.500	0.001	1.999	0.40	2.0	–	–	flat	0.1	15.00	0.8	–
2.6	1.500	0.001	1.999	0.40	2.0	–	–	flat	1.0	15.00	0.8	–
2.7	1.500	0.001	1.999	0.40	2.0	–	–	flat	10.0	15.00	0.8	–
2.8	1.500	0.001	1.999	0.40	2.0	–	–	flat	100.0	15.00	0.8	–
2.9	1.500	0.200	1.800	0.44	2.0	–	–	flat	10.0	15.00	0.8	–
Non-adiabatic with Total Initial Mass = $2M_\odot$ and Total Final Mass = $0.8M_\odot$												
2.11	1.500	0.001	1.999	0.40	2.0	2.98	0.10	equation (51)	42.11	1000	0.5	0°
2.12	1.500	0.001	1.999	0.40	2.0	2.98	0.10	equation (51)	42.11	1000	0.5	45°
2.13	1.500	0.001	1.999	0.40	2.0	2.89	0.10	equation (51)	42.11	1000	0.5	90°
2.14	1.500	0.001	1.999	0.40	2.0	14.89	0.50	equation (51)	42.11	1000	0.5	135°
2.15	1.500	0.001	1.999	0.40	2.0	14.89	0.50	equation (51)	42.11	1000	0.5	180°
2.16	1.500	0.001	1.999	0.40	2.0	14.89	0.50	equation (51)	42.11	1000	0.5	225°
2.17	1.500	0.001	1.999	0.40	2.0	28.29	0.95	equation (51)	42.11	1000	0.5	270°
2.18	1.500	0.001	1.999	0.40	2.0	28.29	0.95	equation (51)	42.11	1000	0.5	315°
2.19	1.500	0.200	1.800	0.44	2.0	26.84	0.95	equation (51)	39.96	1000	0.5	20°

18 models, the secondary is close enough to the star such that the adiabatic approximation may be used. In the last 9 models this approximation does not hold and the general equations are used. The secondary in the first 9 models roughly represents a Kuiper Belt Object such as Pluto. In the remaining models, the secondary mass is approximately equal to that of either Jupiter or a $0.2M_\odot$ star. In all models, we choose semi-major axes and eccentricities such that the secondary's pericentre never interacts with the stellar envelope nor approaches it closely enough that tides are likely to become significant. In their Fig. 7, Mustill & Villaver (2012) demonstrate that for low eccentricity orbits ($e \lesssim 0.2$) the maximum planet radius for which a planet becomes tidally engulfed is located at or within the maximum stellar radius achieved for terrestrial-mass or Neptune-mass planets, but not Jovian-mass planets. The Jovian-mass planets may be enveloped at distances of approximately 3.5 au or 2.7 au if they orbit stars with progenitor masses that are approximately equal to $2M_\odot$ and $1M_\odot$, respectively. However, tidal effects for moderately and highly eccentric cases ($e \gtrsim 0.2$) are poorly constrained, because tidal theories often rely on low-eccentricity expansions.

The quantity t_f present in the table represents the total

time during which a star experiences k times as much mass loss from the eastern hemisphere as the western hemisphere, as in equation (59). We choose this scenario because (1) in the physically-motivated scenario, where both $k = 1$ and u satisfies equation (51), the anisotropic terms make zero contribution to the planet's motion. This result demonstrates the excellence of the isotropic mass-loss approximation. Therefore, we must somehow depart from this scenario. (2) By instead considering a north-south dichotomy in the star, as in equation (55), we would not be able to quantify the change in a or e due to the anisotropic terms because $P_x = P_y = 0$ (see equations 35–36). (3) The adiabatic equations (equations 44–45) admit a closed, analytical solution for $e(t)$ if we assume that both the mass-loss rate and ejecta velocity are constant. Because the solution is similar to equations (A7)–(A9), but with a dependence on k and Heaviside step functions, the equations and numerical simulations can be used to check each other. Subsequently, the analytical equations may be used to quickly model over 10^5 orbits of a planetary companion, such as models 2.1–2.4. (4) Anisotropic behaviour is likely to be transient and averaged out given enough time. Therefore, by presenting an extreme sce-

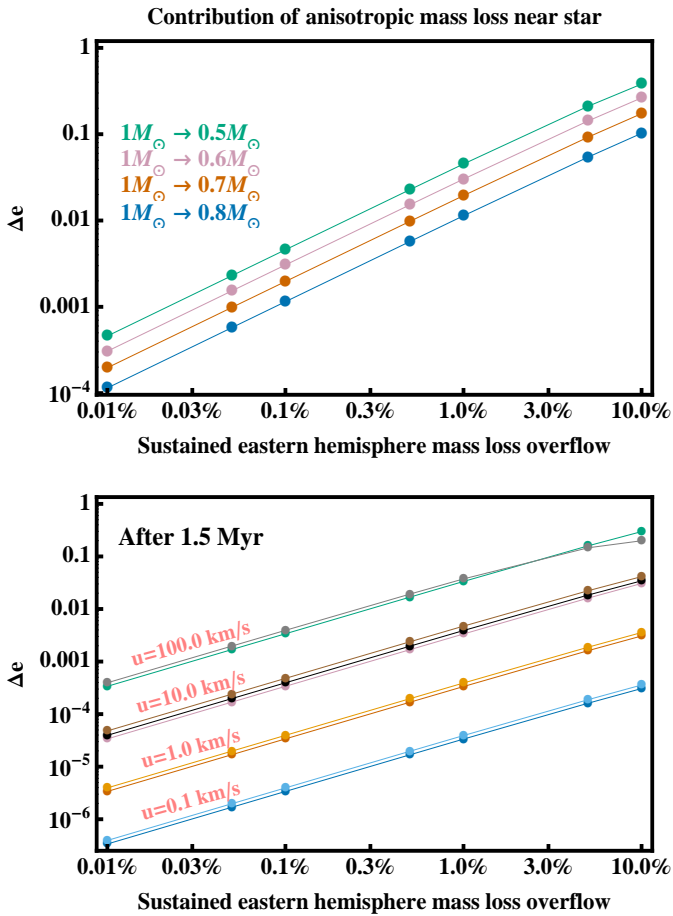


Figure 2. Assessing the robustness of the isotropic mass-loss approximation in post-MS studies. Plotted is the adiabatic change in a secondary’s eccentricity versus $k - 1$ due to the excess mass fraction lost from the eastern hemisphere. We use the anisotropic mass-loss prescription of equation (59). In the upper panel, the blue (bottom) curve represents models 1.1 and 1.5 from Table 1. Moving up, the orange curve represents models 1.2 and 1.6, the purple curve models 1.3 and 1.7, and the green curve models 1.4, 1.8 and 1.9. In the lower panels, the curves from bottom to top represent models 2.1, 2.5, 2.2, 2.6, 2.3, 2.7, 2.9, 2.4 and 2.8. These plots demonstrate that anisotropic mass loss must be sustained at least at the 1 per cent level over at least 1 Myr to produce an observable difference from the isotropic mass-loss case.

nario such as sustained mass loss from one hemisphere, we are presenting an upper bound on the effects of anisotropy.

Consider first the 18 adiabatic models (models 1.1–2.9). In the adiabatic isotropic mass loss case e remains fixed and a varies, whereas in the anisotropic case e varies and a incurs no additional variation. Therefore, the eccentricity achieved in the anisotropic case is due entirely to the anisotropic terms. Consequently, in Fig. 2, we plot Δe as a function of $k - 1$ for models 1.1–1.9 (upper panel) and models 2.1–2.9 (lower panel). Dots represent the outcome of numerical simulations for specific values of k . In the upper panel, we find that the different values of t_f chosen make no discernible difference to the outcome for the same total mass loss. In other words, models 1.1 and 1.5 yield the same result, as do models 1.2 and 1.6, 1.3 and 1.7, and 1.4 and 1.8 and 1.9. In the lower panel all 9 models produce distinct curves on the plot. However, these are sharply grouped

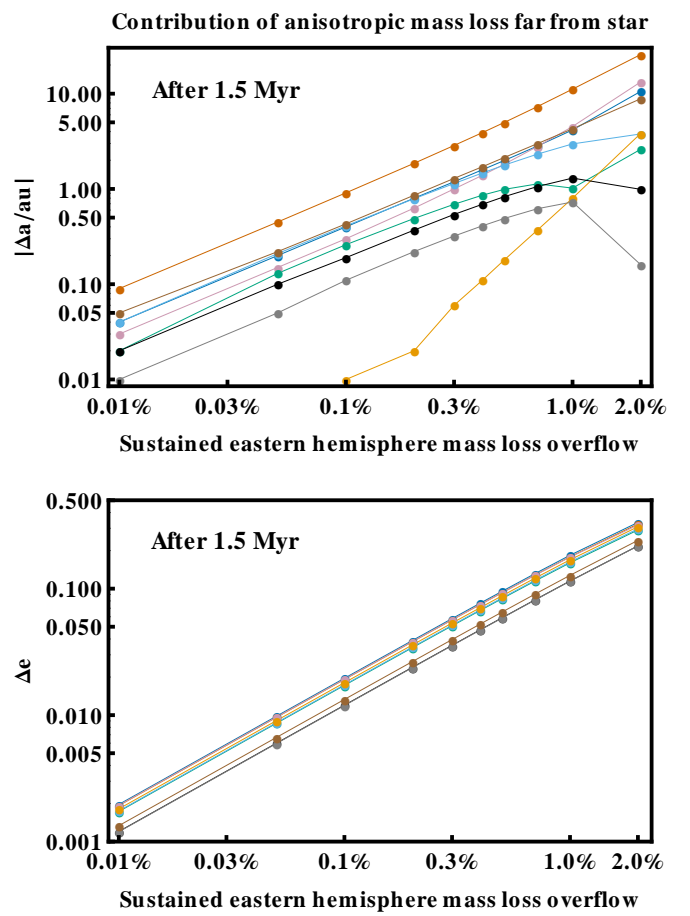


Figure 3. Like Fig. 2 but for the non-adiabatic case, where the secondary is at $a(0) = 10^3$ au. Anisotropic mass-loss has a greater effect in the outer reaches of planetary systems.

according to ejecta velocity. One order of magnitude difference in a uniform ejecta velocity roughly corresponds to one order of magnitude difference in the secondary’s eventual eccentricity. In contrast, when the secondary is a small star (brown curve, third from top), with a mass about two orders of magnitude greater than Jupiter’s mass, the eccentricity increases by just a few tens of percent. Similarly, a 0.7 change in the initial eccentricity makes little difference relative to changes in u . The primary difference is the kink seen for the grey curve ($e_0 = 0.8$) at $k = 1.100$; as the eccentricity approaches unity, de/dt slows.

Now consider the 9 non-adiabatic models (2.11–2.19). In this case, anisotropy affects both a and e , the upper and lower panels of Fig. 3. The behaviour is more complex in the general case because of the dependence on f . This dependence in the isotropic case is discussed in detail by Veras et al. (2011) and Veras & Wyatt (2012). Here we are just interested in the change due to anisotropy. The upper plot shows non-monotonic curves, as well as instances when Δa may reach about 1 per cent of $a(0)$. The magnitude of the eccentricity change for these $a(0) = 1000$ au models for a given k is greater than for the corresponding models in Fig. 2. This comparison corroborates the effect of the extra factor of \sqrt{a} in the anisotropic terms. Nevertheless, the eccentricity still appears to increase uniformly, as in the adiabatic case, despite the introduction of latitudinal dependence on u . These plots confirm the finding of Parriott & Alcock (1998)

that anisotropic mass loss is important primarily in the outer reaches of planetary systems.

Overall, these scenarios quantify the extent to which sustained, strong anisotropic mass loss is necessary in order to produce an observable change in a secondary's orbital parameters.

3.1.4 Complex behaviour of giant stars

We have demonstrated that giant-star anisotropic mass loss may be a strong function of V_{rot} . Our giant star applications in this work established bounds on the strength of the asymmetry with simple assumptions about rotation and mass flux. In reality, these attributes are complex and time dependent, but largely unknown.

In particular, arguments appealing to the conservation of angular momentum in AGB stars – which would dramatically spin down the expansive envelope – largely fail to fit with the dominant fraction of observed planetary nebulae that are aspherical (Kimeswenger et al. 2008). Additionally, despite observations that rapidly rotating AGB stars are classified as very rare (Pereira & Roig 2006), one exception, that of V Hya (Barnbaum et al. 1995), rotates at nearly critical velocity. This rapid rotation may be explained by a binary origin for the star. Another exception mentioned is ZNG 1, which has a measured rotational velocity of $170 \pm 20 \text{ km s}^{-1}$ (Dixon et al. 2004). Dijkstra & Speck (2006) discuss the sources and sinks of angular momentum which can break the assumption of conservation. Although differential rotation has been observed in giant stars (Mosser et al. 2012), observations cannot yet pinpoint the particular form of the angular momentum distribution inside horizontal branch stars. See Sills & Pinsonneault (2000) for four potential angular momentum distributions. Also, see fig. 7 of Heger & Langer (1998) for a sample of rotation profiles due to different assumptions about the internal structure of supergiants.

A complicating factor for mass flux is how the mass loss changes owing to thermal pulses on the AGB. One of the few observational examples of AGB mass loss is due to the spectacular shell of dust and gas around R Sculptoris (Maercker et al. 2012). This shell was created from ejecta from a single thermal pulse. The authors estimate that the pre-pulse, intra-pulse, and post-pulse mass-loss rates over about 200 yr were on the order of, respectively, $10^{-6} M_{\odot} \text{yr}^{-1}$, $10^{-5} M_{\odot} \text{yr}^{-1}$, and $10^{-7} M_{\odot} \text{yr}^{-1}$. Hence, the observations indicate a difference of about 2 orders of magnitude in mass loss on the order of 100 yr for just a single pulse.

The overall lesson from these studies is that, in order to model individual systems where observations fail to provide constraints, one should consider a wide variety of parameters.

3.2 Birth Jets

Currently observed exoplanets orbiting MS stars may have been affected by perturbations due to stellar outflows during their formation. In this section, we quantify how a planet's orbital parameters may have changed.

3.2.1 Context and Assumptions

Unlike in the post-MS case, where mass loss alone affects the orbit of a planet outside of the tidal reach of the parent star, in the

pre-MS case multiple entities may perturb a planet. However, identifying the potential presence and influence of the protoplanetary disc, accretion on to the star, and the release valves for outflows *after* a planet has been formed from that disc is challenging.

The transition between the end of star formation (e.g. Hartmann 1998; McKee & Ostriker 2007) and the beginning of planet formation (e.g. Armitage 2010) is murky, and both processes are not mutually exclusive. Only a handful of authors have attempted to bridge this gap (e.g. Larson 2002; Griv 2007) although there exists an acknowledgment that the presence of planets can affect the accretion rate on to the star (e.g. Goodman & Rafikov 2001; Nayakshin & Lodato 2012; Nayakshin 2013). Therefore, questioning whether a young system with bipolar outflows can plausibly host a fully-formed planet is valid. The formation of bipolar jets themselves (Blandford & Payne 1982; Pudritz & Norman 1983) is a hallmark of accretion on to protostars, and hence a disc often, but not necessarily always⁴, accompanies jets. The proportion of the disc which is dissipated due to accretion, photoevaporation and planet formation, as a function of time, remains unknown both observationally and theoretically.

Nevertheless, this picture may be constrained. In some cases, accretion rates on to the star as high as $5 \times 10^{-7} M_{\odot} \text{yr}^{-1}$ can persist for 1 Myr, and accretion rates as high as $10^{-8} M_{\odot} \text{yr}^{-1}$ can persist for 10 Myr, after the star is born (fig. 7 of Armitage et al. 2003). These lifetimes are commensurate with those of protoplanetary discs (fig. 2 of Wyatt 2008), which place hard constraints on the timescale for planet formation. Stars that react to accretion from discs by expelling matter do so through X-winds (e.g. Shu et al. 1994, 2000; Shang et al. 2007) at inner disc edges (Cai 2009), which typically reside at hundredths of au, or through disc-winds (Konigl & Pudritz 2000; Pudritz et al. 2007) at tenths of an au to several au (e.g. Anderson et al. 2003). The mass accretion rate is typically one order of magnitude higher than the mass ejection rate (Cabrit et al. 1990; Hartigan et al. 1995; Hartmann 1998; Pudritz et al. 2007).

The dual processes of mass accretion and mass ejection may both strongly affect an orbiting planet. However, the ejected mass is being ejected from the system, whereas the accreted mass is being transposed within the system. Therefore, due to accretion, a planet which is external to the accretion disc shifts its orbit only to the extent that the central star has effectively changed its moment of inertia. The planet's osculating Keplerian parameters are not able to undergo the major changes which can accompany mass loss from the system. The further away the planet resides from the disc, the smaller the effect from accretion. Henceforth, we neglect mass accretion in our computations.

The disc itself provides another perturbation on the planet (and vice versa). Namouni (2005) and Namouni (2013), who also consider the effect on planets of bipolar jets, neglect the disc mass. We similarly neglect the disc, but first provide some more detailed justification for doing so. Protoplanetary discs, which are gas-poor remnants of protostellar discs, have observed disc masses ranging from, for example, $10^{-3} - 10^{-1} M_{\odot}$ (fig. 1 of Williams & Cieza 2011).

⁴ Scholz et al. (2013) describe potential disc-based and protoplanet-based triggers of accretion in their introduction.

Given these typical disc masses, we can compute the ratio of the gravitational potential, ψ , of the disc to the total potential (from the disc and star) at arbitrary planet locations. We demonstrate that this ratio is small. We utilize the general potential formulae of Huré (2012), and consider two cases. The first is when the planet is coplanar to the disc and the second is when the planet-star line is perpendicular to the disc. The disc is assumed to be a thin circular annulus extending from 0.05 au to an arbitrary distance R'_d . Then

$$\psi_{\text{disc,coplanar}} = \psi(R_d^{(c)} = R'_d) - \psi(R_d^{(c)} = 0.05 \text{ au}),$$

$$\psi_{\text{disc,vertical}} = \psi(R_d^{(v)} = R'_d) - \psi(R_d^{(v)} = 0.05 \text{ au}),$$

where

$$\psi(R_d^{(c)}) = -2G\Sigma$$

$$\times \left[\left(R_d^{(c)} + R_p \right) \int_0^{\frac{\pi}{2}} \left(1 - \frac{4R_d^{(c)}R_p}{\left(R_d^{(c)} + R_p \right)^2} \sin^2 \zeta \right)^{\frac{1}{2}} d\zeta \right. \\ \left. + \left(R_d^{(c)} - R_p \right) \int_0^{\frac{\pi}{2}} \left(1 - \frac{4R_d^{(c)}R_p}{\left(R_d^{(c)} + R_p \right)^2} \sin^2 \zeta \right)^{-\frac{1}{2}} d\zeta \right], \quad (65)$$

$$\psi(R_d^{(v)}) = -2\pi G\Sigma \left[\sqrt{R_d^{(v)2} + R_p^2} - R_d^{(v)} \right] \quad (66)$$

and Σ is the disc surface density, which we assume to be a power law. In Fig. 4, we plot the results for $R'_d = 1$ au and two power-law exponents. For each pair of similarly-coloured curves, the top represents the Keplerian power law exponent ($-3/2$) and the bottom represents a linear exponent (-1).

For all curves, the disc contribution to the potential never reaches a tenth, and achieves a hundredth only when $M_{\text{disc}} > 0.01M_s$. Both cases presented are broadly similar, and do include feedback on the disc. As expected, the disc contribution becomes asymptotic for large R_p and approaches zero as $R_p \rightarrow 0$. Because of this asymptotic behaviour, when modelling an external planet affected by jet-induced mass ejection, one may simply add the stellar mass to the disc mass and treat both as a single entity.

In summary, we believe the assumptions of Namouni (2013) of neglecting accretion and influences from the disc are valid for the precision sought. We make the same assumptions in the subsequent analysis.

3.2.2 General Jets

In Appendix A, we consider the movement of a planet caused by a jet of material emanating from the star in an arbitrary direction. The equations there also incorporate the mass loss expected from the rest of the star along with the jet.

3.2.3 Asymmetric Bipolar Jets

One physically-motivated case of particular interest is bipolar jets. In the limit of infinitesimally thin jets which contain all the stellar mass loss, there is no longitudinal dependence on mass-loss, and hence $P_x = P_y = 0$. Therefore $F_x = Q_{13}P_z$, $F_y = Q_{23}P_z$ and $F_z = Q_{33}P_z$. When both jets are completely symmetric, they eject mass at the same rate and velocity, so

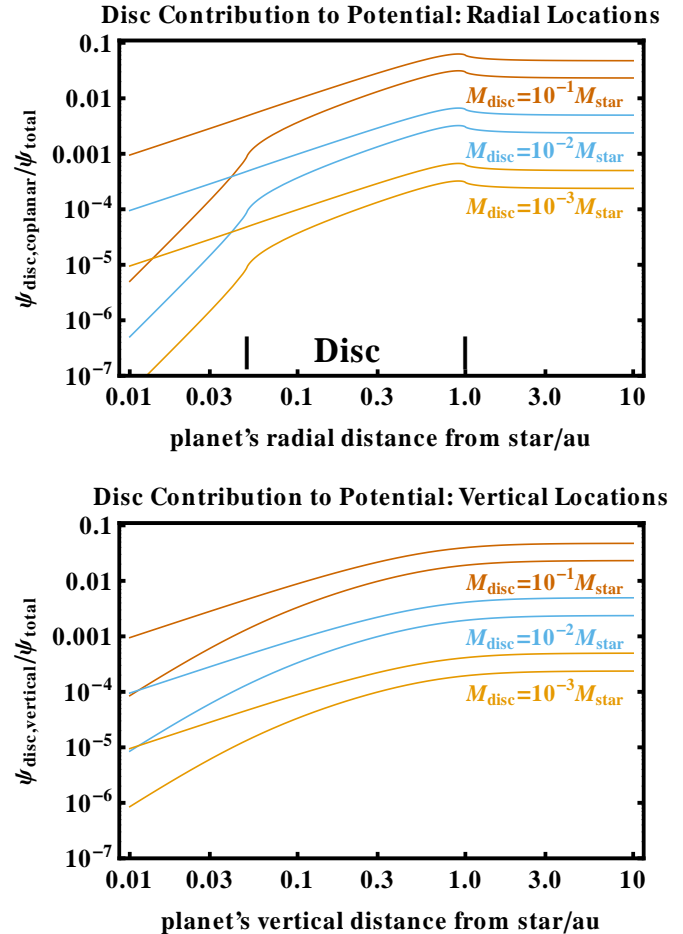


Figure 4. A demonstration of why accretion discs may be neglected for nascent system mass loss studies. The top and bottom plots show the fraction of the total gravitational potential on a planet due to a thin disc annulus from 0.05 - 1.0 au for radial and polar planet locations, respectively. For each pair of curves, the top and bottom assume r^{-1} and $r^{-3/2}$ mass distributions in the disc.

there is no net anisotropic force on the planet *regardless of the planet's location*.

Consider ideal asymmetric bipolar jets which do produce a net anisotropic force on a planetary orbit. We can deduce several properties of the resulting motion just by considering equations (35)–(39) and equations (44)–(48), with $P_x = P_y = 0$. The reduced form of equations (44)–(48) has the following properties.

- 1) A planet's eccentricity remains fixed, just as in the isotropic adiabatic mass-loss case.
- 2) An eccentric planet has an argument of pericentre that precesses continuously unless $\omega_0 = 0$.
- 3) The magnitudes of di/dt , $d\Omega/dt$ and $d\omega/dt$ all correlate positively with eccentricity.

We analyze the case $\omega_0 = 0$ in the adiabatic regime because this case admits complete analytical solutions for the orbit. The resulting motion demonstrates how the semimajor axis and inclination evolve with a static eccentricity. Let us denote the mass-loss rate and velocity at $\theta = 0$ and $\theta = \pi$ as $\{\dot{M}_{\text{up}} > 0, u_{\text{up}} > 0\}$ and $\{\dot{M}_{\text{down}} > 0, u_{\text{down}} > 0\}$, and treat these quantities as constant in time. Hence, we solve

Table 2. Model parameters for Figs. 5-6. Here, \dot{M}_{up} , \dot{M}_{down} , u_{up} and u_{down} refer to the mass loss rate and outflow velocity at the north pole ($\theta = 0$, “up”) and south pole ($\theta = \pi$, “down”).

Model #	$\frac{M_p}{M_\odot}$	$\frac{M_s(0)}{M_\odot}$	$\frac{\dot{M}_{\text{up}}}{M_\odot/\text{yr}}$	$\frac{\dot{M}_{\text{down}}}{M_\odot/\text{yr}}$	$\frac{u_{\text{up}}}{\text{km/s}}$	$\frac{u_{\text{down}}}{\text{km/s}}$	$\frac{a(0)}{\text{au}}$	e
Adiabatic with Total Initial Mass = $1M_\odot$								
J1.1	0.001	0.999	1×10^{-10}	2×10^{-10}	10	20	5.0	0.5
J1.2	0.001	0.999	1×10^{-10}	2×10^{-10}	100	200	5.0	0.5
J1.3	0.001	0.999	1×10^{-10}	4×10^{-10}	100	200	5.0	0.5
J1.4	0.001	0.999	1×10^{-8}	2×10^{-8}	10	20	5.0	0.5
J1.5	0.001	0.999	1×10^{-8}	2×10^{-8}	100	200	5.0	0.5
J1.6	0.001	0.999	1×10^{-8}	4×10^{-8}	100	200	5.0	0.5
J1.7	0.001	0.999	1×10^{-6}	2×10^{-6}	10	20	5.0	0.5
J1.8	0.001	0.999	1×10^{-6}	2×10^{-6}	100	200	5.0	0.5
J1.9	0.001	0.999	1×10^{-6}	4×10^{-6}	100	200	5.0	0.5
Adiabatic with Total Initial Mass = $2M_\odot$								
J2.1	0.001	1.999	4×10^{-7}	5×10^{-7}	50	75	1.0	0.01
J2.2	0.001	1.999	4×10^{-7}	5×10^{-7}	50	75	1.0	0.2
J2.3	0.001	1.999	4×10^{-7}	5×10^{-7}	50	75	1.0	0.7
J2.4	0.001	1.999	4×10^{-7}	5×10^{-7}	50	75	3.0	0.01
J2.5	0.001	1.999	4×10^{-7}	5×10^{-7}	50	75	3.0	0.2
J2.6	0.001	1.999	4×10^{-7}	5×10^{-7}	50	75	3.0	0.7
J2.7	0.001	1.999	4×10^{-7}	5×10^{-7}	50	75	10.0	0.01
J2.8	0.001	1.999	4×10^{-7}	5×10^{-7}	50	75	10.0	0.2
J2.9	0.001	1.999	4×10^{-7}	5×10^{-7}	50	75	10.0	0.7

$$\frac{da}{dt} = -\frac{a(t)}{M_s(t) + M_p} (\dot{M}_{\text{up}} + \dot{M}_{\text{down}}), \quad (67)$$

$$\begin{aligned} \frac{di}{dt} &= \frac{3e}{2M_s(t)\sqrt{1-e^2}} \sqrt{\frac{a(t)}{G(M_s(t) + M_p)}} \\ &\times (\dot{M}_{\text{down}}u_{\text{down}} - \dot{M}_{\text{up}}u_{\text{up}}). \end{aligned} \quad (68)$$

Recall that the eccentricity is constant. For a finite secondary mass, the solutions to equations (67)–(68) are

$$M_s(t) = M_s(0) - t(\dot{M}_{\text{up}} + \dot{M}_{\text{down}}), \quad (69)$$

$$a(t) = a(0) \frac{M_s(0) + M_p}{M_s(0) + M_p - t(\dot{M}_{\text{up}} + \dot{M}_{\text{down}})}, \quad (70)$$

$$\begin{aligned} i(t) &= i(0) - \frac{3e}{2\sqrt{1-e^2}} \left(\frac{\dot{M}_{\text{down}}u_{\text{down}} - \dot{M}_{\text{up}}u_{\text{up}}}{\dot{M}_{\text{down}} + \dot{M}_{\text{up}}} \right) \\ &\times \sqrt{\frac{a(0)(M_s(0) + M_p)}{GM_p^2}} \\ &\times \ln \left(\frac{(M_s(0) + M_p) [M_s(0) - t(\dot{M}_{\text{down}} + \dot{M}_{\text{up}})]}{M_s(0) [M_s(0) + M_p - t(\dot{M}_{\text{down}} + \dot{M}_{\text{up}})]} \right), \end{aligned} \quad (71)$$

whereas the inclination solution for a test particle secondary is instead

$$i(t) = i(0) - \frac{3e}{2\sqrt{1-e^2}} \sqrt{\frac{a(0)}{GM_s(0)}} \left(\frac{\dot{M}_{\text{down}}u_{\text{down}} - \dot{M}_{\text{up}}u_{\text{up}}}{\dot{M}_{\text{down}} + \dot{M}_{\text{up}}} \right). \quad (72)$$

The solutions show that an eccentric secondary's semimajor axis and inclination both *evolve monotonically with time*. Therefore, the orbital plane always moves towards a pole unless

the orbit is circular. The higher the eccentricity, the faster this movement. If the jet at the south pole is stronger than that at the north pole ($\dot{M}_{\text{down}}u_{\text{down}} > \dot{M}_{\text{up}}u_{\text{up}}$), then the inclination always decreases. The greater the asymmetry, the faster the inclination changes. Also, although the eccentricity remains static, the location of the pericentre is a function of time.

3.2.4 Specific Examples

Now we consider specific, observationally-motivated examples. The time-dependent mass-loss rates and velocities of these jets are unknown. Therefore, let us remove the time dependence of J and u in the following examples. We now seek to obtain observational constraints, including differences between the north and south jets.

For the stellar mass range of interest here ($M_\odot \lesssim 7M_\odot$), we find representative ranges of mass-loss rates of $10^{-10} - 10^{-6}M_\odot/\text{yr}$ and ejection velocities of tens to hundreds of km s^{-1} . We obtained these ranges by considering specific examples of observed jets given in table 4 of Podio et al. (2006), table 3 of Coffey et al. (2008), table 1 of Melnikov et al. (2008), table 1 of Podio et al. (2011), and table 5 of Ellerbroek et al. (2013)⁵. The observed differences in velocities between both jet components vary but may be approximated by a factor of about two. This factor agrees with the estimate of Namouni (2013) and his references. The asymmetry in the mass-loss rate may similarly be approximated by a factor of a few.

These considerations lead us to select the set of models in table 2. The first 9 models feature jets for which the difference

⁵ For more massive stars, typical mass-loss rates often exceed $10^{-5}M_\odot\text{yr}^{-1}$ (see table 2 of Cesaroni et al. 2007).

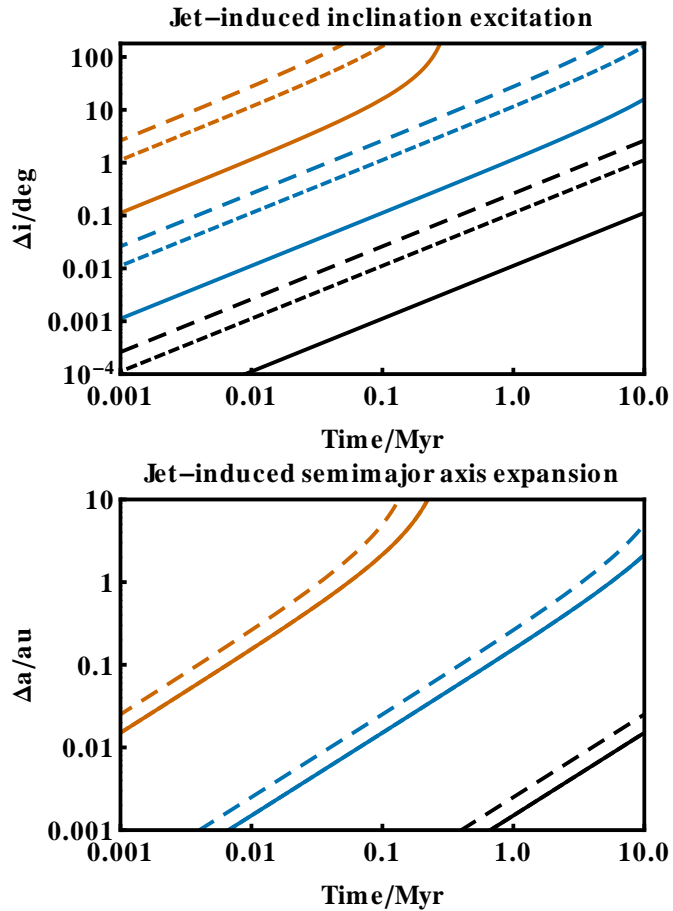


Figure 5. How asymmetric bipolar jets tilt and expand an orbit. The plots illustrate the change in the planet’s inclination (*upper panel*) and semimajor axis (*lower panel*) in models J1.1-J1.9 in Table 2. The model number increases monotonically from the bottom curve to the top in the upper panel. In the lower panel the solid and short-dashed curves are equivalent. Curves of the same colour correspond to roughly the same order of magnitude for mass-loss rates. The plots demonstrate that a realistic sample of models can reproduce observed exoplanet inclinations.

between mass-loss rates and ejecta velocities for both components is a factor of 2 or 4. We shrink this factor to 1.25 and 1.50 for the last 9 models. For the first 9 models we also vary the mass-loss rates by 4 orders of magnitude, whereas for the last 9 models we vary the planet’s semimajor axis and eccentricity. In all models $\omega_0 = 0$, so that equations (69)-(71) are satisfied. We checked that the output from those equations agree with output from the full adiabatic set of differential equations. These have further been checked against the output from the non-adiabatic equations for up to 10^4 orbits of the planet.

We plot the resulting semimajor axis and inclination variation in Fig. 5 (for models J1.1-J1.9) and Fig. 6 (for models J2.1-J2.9). These plots illustrate that if the jets are sustained for a long enough period of time, then any inclination may be achieved. Because $\Delta i \propto u$, the faster the ejecta velocity, the less mass which has to be lost in order to achieve the same level of orbital excitation. The semimajor axis evolution is however independent of u because, in the adiabatic case, there is no anisotropic contribution to da/dt (further, more generally in the non-adiabatic case, P_z makes no contribution to da/dt). Other

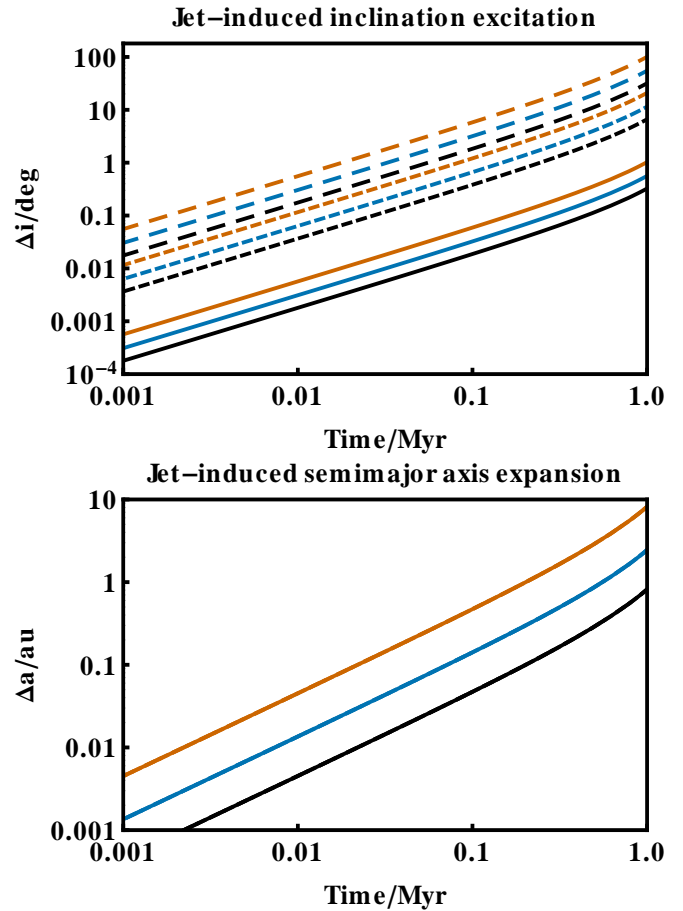


Figure 6. The same as Fig. 5 but for models J2.1-J2.9 in Table 2. There include variations in the initial planetary orbit. In the upper panel, starting at the bottom curve and moving up, the curves correspond to models J2.1, J2.4, J2.7, J2.2, J2.5, J2.8, J2.3, J2.6 and J2.9. Curves of the same colour correspond to the same value of $a(0)$. Hence, because the equivalently-coloured curves are so widely separated, the upper panel demonstrates the strong dependence of $i(t)$ on e .

dependencies apparent in the plots include $\Delta i \propto e/\sqrt{1-e^2}$ and $\Delta i \propto \sqrt{a}$. Fig. 5 illustrates that for $\dot{M} \approx 10^{-8} M_\odot/\text{yr}$, the jets can produce an inclination variation of about one degree in under 1 Myr. More symmetric jets would hamper this excitation, but fail to do so in the models of Fig. 6 because the mass-loss rate is higher by an order of magnitude than that of those of Fig. 5.

Finally we caution that, in the more general case with $\omega_0 \neq 0$, di/dt exhibits more complex behaviour until ω vanishes. Further, in the non-adiabatic case, when a is large (typically exceeding hundreds of au), the inclination evolution does not behave in such a regular fashion.

4 CONCLUSION

We have derived the anisotropic contribution (equations 35–39 and 44–48) to the orbital equations of motion (equations 18–23) for a companion to a primary star that is shedding mass in arbitrary directions with arbitrary velocities. The relative contribution of the anisotropic terms to the overall motion scale as \sqrt{a} . Because this contribution typically vanishes (equations 52–54) for a planet in a post-MS system anywhere within hundreds of au of its parent star, we conclude that the isotropic mass loss approximation is robust for most post-MS planetary studies. Contrastingly, in nascent planetary systems and in the absence of other forces, persistent, asymmetric, sufficiently long-lived bipolar jets may regularly excite exoplanet inclinations to a few degrees.

ACKNOWLEDGEMENTS

This manuscript is dedicated to co-author John D. Hadjidemetriou, whose passing came to light the day after submission. His distinguished career spanned half of a century, and this paper represents a long-planned generalisation of his pioneering 1963 paper results. He will be sorely missed.

We thank the referee for constructive and insightful comments, which have improved the context of the manuscript's content considerably. We also thank Lorenzo Iorio for providing us with a copy of the paper by Omarov (1962), and Alexander J. Mustill and Cathie J. Clarke for useful discussions. CAT thanks Churchill College for his fellowship.

REFERENCES

- Adams, F. C., Anderson, K. R., & Bloch, A. M. 2013, *MNRAS*, 432, 438
- Addison, B. C., Tinney, C. G., Wright, D. J., et al. 2013, arXiv:1306.0878
- Anderson, J. M., Li, Z.-Y., Krasnopolsky, R., & Blandford, R. D. 2003, *ApJL*, 590, L107
- Armitage, P. J. 2010, *Astrophysics of Planet Formation*, by Philip J. Armitage, pp. 294. ISBN 978-0-521-88745-8 (hardback). Cambridge, UK: Cambridge University Press, 2010.,
- Armitage, P. J., Clarke, C. J., & Palla, F. 2003, *MNRAS*, 342, 1139
- Barnbaum, C., Morris, M., & Kahane, C. 1995, *ApJ*, 450, 862
- Blandford, R. D., & Payne, D. G. 1982, *MNRAS*, 199, 883
- Bonsor, A., Mustill, A. J., & Wyatt, M. C. 2011, *MNRAS*, 414, 930
- Bonsor, A., Augereau, J.-C., & Thébault, P. 2012, *A&A*, 548, A104
- Boué, G., Figueira, P., Correia, A. C. M., & Santos, N. C. 2012, *A&A*, 537, L3
- Cabrit, S., Edwards, S., Strom, S. E., & Strom, K. M. 1990, *ApJ*, 354, 687
- Cai, M. J. 2009, *Protostellar Jets in Context*, 143
- Campbell, B., Walker, G. A. H., & Yang, S. 1988, *ApJ*, 331, 902
- Castor, J. I., Abbott, D. C., & Klein, R. I. 1975, *ApJ*, 195, 157
- Catelan, M. 2009, *Ap&SS*, 320, 261
- Cesaroni, R., Galli, D., Lodato, G., Walmsley, C. M., & Zhang, Q. 2007, *Protostars and Planets V*, 197
- Coffey, D., Bacciotti, F., & Podio, L. 2008, *ApJ*, 689, 1112
- Cranmer, S. R., & Owocki, S. P. 1995, *ApJ*, 440, 308
- Debes, J. H., & Sigurdsson, S. 2002, *ApJ*, 572, 556
- Debes, J. H., Walsh, K. J., & Stark, C. 2012, *ApJ*, 747, 148
- Diprit, A. 1983, *Celestial Mechanics*, 31, 1
- Dijkstra, C., & Speck, A. K. 2006, *ApJ*, 651, 288
- Dixon, W. V. D., Brown, T. M., & Landsman, W. B. 2004, *ApJL*, 600, L43
- Ekström, S., Meynet, G., Chiappini, C., Hirschi, R., & Maeder, A. 2008, *A&A*, 489, 685
- Ellerbroek, L. E., Podio, L., Kaper, L., et al. 2013, *A&A*, 551, A5
- Geier, S., Edelmann, H., Heber, U., & Morales-Rueda, L. 2009, *ApJL*, 702, L96
- Georgy, C., Meynet, G., & Maeder, A. 2011, *A&A*, 527, A52
- Gettel, S., Wolszczan, A., Niedzielski, A., et al. 2012, *ApJ*, 745, 28
- Goodman, J., & Rafikov, R. R. 2001, *ApJ*, 552, 793
- Griv, E. 2007, *P&SS*, 55, 547
- Hadjidemetriou, J. D. 1963, *Icarus*, 2, 440
- Hartigan, P., Edwards, S., & Ghandour, L. 1995, *ApJ*, 452, 736
- Hartmann, L. 1998, *Accretion processes in star formation / Lee Hartmann*. Cambridge, UK ; New York : Cambridge University Press, 1998. (Cambridge astrophysics series ; 32) ISBN 0521435072.,
- Hatzes, A. P., Guenther, E. W., Endl, M., et al. 2005, *A&A*, 437, 743
- Heger, A., Langer, N., & Woosley, S. E. 2000, *ApJ*, 528, 368
- Heger, A., & Langer, N. 1998, *A&A*, 334, 210
- Huré, J.-M. 2012, *Celestial Mechanics and Dynamical Astronomy*, 114, 365
- Hurley, J. R., Pols, O. R., & Tout, C. A. 2000, *MNRAS*, 315, 543
- Iorio, L. 2012, *New Astronomy*, 17, 356
- Kimeswenger, S., Zijlstra, A. A., van Hoof, P. A. M., et al. 2008, arXiv:0804.4058
- Konigl, A., & Pudritz, R. E. 2000, *Protostars and Planets IV*, 759
- Langer, N. 1998, *A&A*, 329, 551
- Larson, R. B. 2002, *MNRAS*, 332, 155
- Latham, D. W., Stefanik, R. P., Mazeh, T., Mayor, M., & Burki, G. 1989, *Nature*, 339, 38
- Lee, J. W., Kim, S.-L., Kim, C.-H., Koch, R. H., Lee, C.-U., Kim, H.-I., & Park, J.-H. 2009, *AJ*, 137, 3181
- Li, L.-S. 2008, *Astronomy Reports*, 52, 806
- Lovekin, C. C. 2011, *MNRAS*, 415, 3887
- Maeder, A. 2002, *A&A*, 392, 575
- Maeder, A., & Meynet, G. 2000, *A&A*, 361, 159
- Maercker, M., Mohamed, S., Vlemmings, W. H. T., et al. 2012, *Nature*, 490, 232
- McKee, C. F., & Ostriker, E. C. 2007, *ARA&A*, 45, 565
- Melnikov, S., Woitas, J., Eislöffel, J., et al. 2008, *A&A*, 483, 199
- Mosser, B., Goupil, M. J., Belkacem, K., et al. 2012, *A&A*, 548, A10
- Mullally, F., Winget, D. E., De Gennaro, S., Jeffery, E., Thompson, S. E., Chandler, D., & Kepler, S. O. 2008, *ApJ*, 676, 573
- Mullally, F., Reach, W. T., De Gennaro, S., & Burrows, A. 2009, *ApJ*, 694, 327
- Mustill, A. J., & Villaver, E. 2012, *ApJ*, 761, 121
- Namouni, F. 2005, *AJ*, 130, 280
- Namouni, F. 2013, *Ap&SS*, 343, 53

- Namouni, F., & Guzzo, M. 2007, *Celestial Mechanics and Dynamical Astronomy*, 99, 31
- Namouni, F., & Zhou, J. L. 2006, *Celestial Mechanics and Dynamical Astronomy*, 95, 245
- Nayakshin, S. 2013, *MNRAS*, 431, 1432
- Nayakshin, S., & Lodato, G. 2012, *MNRAS*, 426, 70
- Nordhaus, J., Spiegel, D. S., Ibgui, L., Goodman, J., & Burrows, A. 2010, *MNRAS*, 408, 631
- Nordhaus, J., & Spiegel, D. S. 2013, *MNRAS*, 432, 500
- Omarov, T. B. 1962, *Izv. Astrofiz. Inst. Acad. Nauk. KazSSR*, 14, 66
- Omarov, T. B. 1964, *Soviet Astronomy*, 8, 127
- Owocki, S. P., Cranmer, S. R., & Gayley, K. G. 1996, *ApJL*, 472, L115
- Owocki, S. P., Cranmer, S. R., & Gayley, K. G. 1998, *Ap&SS*, 260, 149
- Parriott, J., & Alcock, C. 1998, *ApJ*, 501, 357
- Passy, J.-C., Mac Low, M.-M., & De Marco, O. 2012, *ApJL*, 759, L30
- Pereira, C. B., & Roig, F. 2006, *A&A*, 452, 571
- Podio, L., Bacciotti, F., Nisini, B., et al. 2006, *A&A*, 456, 189
- Podio, L., Eisloffel, J., Melnikov, S., Hodapp, K. W., & Bacciotti, F. 2011, *A&A*, 527, A13
- Pudritz, R. E., & Norman, C. A. 1983, *ApJ*, 274, 677
- Pudritz, R. E., Ouyed, R., Fendt, C., & Brandenburg, A. 2007, *Protostars and Planets V*, 277
- Puls, J., Vink, J. S., & Najarro, F. 2008, *A&AR*, 16, 209
- Rahoma, W. A., Abd El-Salam, F. A., & Ahmed, M. K. 2009, *Journal of Astrophysics and Astronomy*, 30, 187
- Sato, B., Omiya, M., Harakawa, H., et al. 2012, *PASJ*, 64, 135
- Scholz, A., Froebrich, D., & Wood, K. 2013, *MNRAS*, 430, 2910
- Setiawan, J., Klement, R. J., Henning, T., Rix, H.-W., Rochau, B., Rodmann, J., & Schulze-Hartung, T. 2010, *Science*, 330, 1642
- Shang, H., Li, Z.-Y., & Hirano, N. 2007, *Protostars and Planets V*, 261
- Shu, F., Najita, J., Ostriker, E., et al. 1994, *ApJ*, 429, 781
- Shu, F. H., Laughlin, G., Lizano, S., & Galli, D. 2000, *ApJ*, 535, 190
- Sigurdsson, S., Richer, H. B., Hansen, B. M., Stairs, I. H., & Thorsett, S. E. 2003, *Science*, 301, 193
- Sills, A., & Pinsonneault, M. H. 2000, *ApJ*, 540, 489
- Silvotti, R., et al. 2007, *Nature*, 449, 189
- Spiegel, D. S. 2012, arXiv:1208.2276
- Varvoglis, H., & Hadjidemetriou, J. D. 2012, *Ap&SS*, 339, 207
- Vassiliadis, E., & Wood, P. R. 1993, *ApJ*, 413, 641
- Veras, D., & Evans, N.W. 2013, *Celestial Mechanics and Dynamical Astronomy*, 115, 123
- Veras, D., Mustill, A. J., Bonsor, A., & Wyatt, M. C. 2013, *MNRAS*, 431, 1686
- Veras, D., & Tout, C. A. 2012, *MNRAS*, 422, 1648
- Veras, D., & Wyatt, M. C. 2012, *MNRAS*, 421, 2969
- Veras, D., Wyatt, M. C., Mustill, A. J., Bonsor, A., & Eldridge, J. J. 2011, *MNRAS*, 417, 2104
- Verhulst, F. 1969, *BAIN*, 20, 215
- Villaver, E. 2011, *American Institute of Physics Conference Series*, 1331, 21
- Villaver, E., & Livio, M. 2007, *ApJ*, 661, 1192
- Villaver, E., & Livio, M. 2009, *ApJL*, 705, L81
- von Zeipel, H. 1924, *MNRAS*, 84, 665
- Voyatzis, G., Hadjidemetriou, J. D., Veras, D., & Varvoglis, H. 2013, *MNRAS*, 430, 3383
- Wickramasinghe, D. T., Farihi, J., Tout, C. A., Ferrario, L., & Stancliffe, R. J. 2010, *MNRAS*, 404, 1984
- Williams, J. P., & Cieza, L. A. 2011, *ARA&A*, 49, 67
- Winn, J. N., Johnson, J. A., Albrecht, S., et al. 2009, *ApJL*, 703, L99
- Wolszczan, A., & Frail, D. A. 1992, *Nature*, 355, 145
- Wyatt, M. C. 2008, *ARA&A*, 46, 339
- Zhou, G., & Huang, C. X. 2013, arXiv:1307.2249

APPENDIX A:

Here we derive the equations of motion for a jet outflow of mass in an arbitrary direction, coupled with the background isotropic mass-loss from the star. Suppose the star is losing mass with a realistic flux rate and velocity given by equations (49)-(51) everywhere except in a solid angle bounded by $0 \leq \theta_1 \leq \theta \leq \theta_2 \leq \pi$ and $0 \leq \phi_1 \leq \phi \leq \phi_2 \leq 2\pi$. In this region, the mass-loss rate is constant and uniform and is enhanced from J_0 by a factor of k_J . Similarly, the ejecta velocity is constant and uniform and is enhanced from the polar value $u_0 \equiv u(\theta = 0)$ by a factor of k_u . Then

$$\begin{aligned} P_x &= \frac{u_0 J_0}{4\pi} \left[\int_0^{\phi_1} \cos \phi d\phi \int_0^{\theta_1} (1 - T \sin^2 \theta)^{\frac{3}{2}} \sin \theta d\theta + k_u k_J \int_{\phi_1}^{\phi_2} d\phi \int_{\theta_1}^{\theta_2} d\theta + \int_{\phi_2}^{2\pi} \cos \phi d\phi \int_{\theta_2}^{\pi} (1 - T \sin^2 \theta)^{\frac{3}{2}} \sin \theta d\theta \right] \\ &= \frac{u_0 J_0}{4\pi} \left\{ k_u k_J (\theta_1 - \theta_2) (\phi_1 - \phi_2) + \frac{1}{16} \sin \phi_1 [S_{1-}(\theta_1) + S_{2+}(\theta_1)] - \frac{1}{16} \sin \phi_2 [S_{1+}(\theta_2) - S_{2-}(\theta_2)] \right\}, \end{aligned} \quad (\text{A1})$$

$$\begin{aligned} P_y &= \frac{u_0 J_0}{4\pi} \left[\int_0^{\phi_1} \sin \phi d\phi \int_0^{\theta_1} (1 - T \sin^2 \theta)^{\frac{3}{2}} \sin \theta d\theta + k_u k_J \int_{\phi_1}^{\phi_2} d\phi \int_{\theta_1}^{\theta_2} d\theta + \int_{\phi_2}^{2\pi} \sin \phi d\phi \int_{\theta_2}^{\pi} (1 - T \sin^2 \theta)^{\frac{3}{2}} \sin \theta d\theta \right] \\ &= \frac{u_0 J_0}{4\pi} \left\{ k_u k_J (\theta_1 - \theta_2) (\phi_1 - \phi_2) + \frac{1}{16} (1 - \cos \phi_1) [S_{1-}(\theta_1) + S_{2+}(\theta_1)] - \frac{1}{16} (1 - \cos \phi_2) [S_{1+}(\theta_2) - S_{2-}(\theta_2)] \right\}, \end{aligned} \quad (\text{A2})$$

$$\begin{aligned} P_z &= \frac{u_0 J_0}{4\pi} \left[\int_0^{\phi_1} d\phi \int_0^{\theta_1} (1 - T \sin^2 \theta)^{\frac{3}{2}} \cos \theta d\theta + k_u k_J \int_{\phi_1}^{\phi_2} d\phi \int_{\theta_1}^{\theta_2} d\theta + \int_{\phi_2}^{2\pi} d\phi \int_{\theta_2}^{\pi} (1 - T \sin^2 \theta)^{\frac{3}{2}} \cos \theta d\theta \right] \\ &= \frac{u_0 J_0}{4\pi} \{ k_u k_J (\theta_1 - \theta_2) (\phi_1 - \phi_2) + \phi_1 S_3(\theta_1) - (2\pi - \phi_2) S_3(\theta_2) \}, \end{aligned} \quad (\text{A3})$$

where, with approximations at small T ,

$$S_{1\pm}(\theta) = 10 - 6T \pm \cos \theta (5 - 4T + T \cos 2\theta) \sqrt{4 - 2T + 2T \cos 2\theta} \approx 10 (1 \pm \cos \theta) + \left(-6 \mp \frac{21}{2} \cos \theta \pm \frac{9}{2} \cos \theta \cos 2\theta \right) T,$$

$$S_{2\pm}(\theta) = 6T^{-\frac{1}{2}} (T - 1)^2 \ln \left[\frac{\sqrt{2} \pm \sqrt{2T}}{\sqrt{2T} \cos \theta + \sqrt{2 - T + T \cos 2\theta}} \right] \approx 6 (\pm 1 - \cos \theta) + \sin^2 \left(\frac{\theta}{2} \right) (\mp 21 + 2 \cos \theta \mp \cos 2\theta) T,$$

$$S_3(\theta) = 3T^{-\frac{1}{2}} \arcsin \left[\sqrt{T} \sin \theta \right] + \sin \theta (5 - 2T \sin^2 \theta) \sqrt{1 - T \sin^2 \theta} \approx 8 \sin \theta - (4 \sin^3 \theta) T.$$

The material emanating in the jet generally is constant in neither k_J nor k_u . In particular, the formation and dissipation of the jet might cause accelerations and decelerations which could affect planetary motion. If all of the stellar mass loss is contained in the jet, then the equations are considerably simplified and retain a single term each. In this situation, $P_x = P_y = P_z$. Similarly, if the vast majority of mass loss is in the jet, then the other terms may be neglected. Additional jets of mass loss may be added on to the above relations by splitting the integrals appropriately.

If there is latitudinal symmetry such that $P_z = 0$ for an ideal jet in the XY plane, then we can attempt to solve the adiabatic equations of motion. Suppose the mass-loss rate of the jet is constant and $\dot{M} > 0$, and the mass is lost at a constant speed $u > 0$. Then, *regardless of the orientation of the jet in the equatorial plane*,

$$\frac{da}{dt} = -\frac{a(t)}{M_s(t) + M_p} \dot{M}, \quad (\text{A4})$$

$$\frac{de}{dt} = -\frac{3\sqrt{1 - e(t)^2}}{2M_s(t)} \sqrt{\frac{a(t)}{G(M_s(t) + M_p)}} u \dot{M}. \quad (\text{A5})$$

These equations admit complete solutions. For a finite secondary mass (including a secondary star), the solutions are

$$M_s(t) = M_s(0) - t\dot{M}, \quad (\text{A6})$$

$$a(t) = a(0) \frac{M_s(0) + M_p}{M_s(0) + M_p - t\dot{M}}, \quad (\text{A7})$$

$$e(t) = \cos \left[2\arcsin \sqrt{\frac{1 - e_0}{2}} - \frac{3u}{2} \sqrt{\frac{a_0 (M_s(0) + M_p)}{GM_p^2}} \ln \left(\frac{M_s(0) [M_s(0) + M_p - t\dot{M}]}{(M_s(0) + M_p) [M_s(0) - t\dot{M}]} \right) \right], \quad (\text{A8})$$

whereas for a test particle

$$e(t) = \cos \left[-2\arcsin \sqrt{\frac{1 - e_0}{2}} + \frac{3ut\dot{M}}{2M_s(0)} \sqrt{\frac{a_0 M_s(0)}{G}} \frac{1}{M_s(0) - \dot{M}t} \right]. \quad (\text{A9})$$

Equation (A7) shows that a secondary's orbit always expands. While doing so, the orbit stretches and contracts, momentarily becoming circular and flat. Equations (A8)-(A9) can be solved analytically for the times at which the orbit becomes momentarily

flat. Depending on the planet's position along its orbit at these times, the planet may be disrupted or destroyed by the central star. Let us consider the first instance in which a test particle will achieve a flat orbit, and denote this time as t_{flat} . We find

$$t_{\text{flat}} = \left(\frac{M_s(0)}{\dot{M}} \right) \left[1 + \frac{3u/V_c(0)}{4\arcsin\sqrt{\frac{1-e_0}{2}}} \right]^{-1} \quad (\text{A10})$$

where the initial circular velocity of the particle is $V_c(0) = \sqrt{GM_s(0)/a_0}$. Equation (A10) demonstrates that t_{flat} is just the time for the star to lose all its mass, modulo a factor that depends on u , $V_c(0)$ and e_0 . In the limit $u \rightarrow 0$ or $V_c(0) \rightarrow \infty$, the factor in square brackets becomes unity, and hence t_{flat} can be reached only if the entire star is dissipated. Alternatively, in the limit $u \rightarrow \infty$, the orbit becomes flat immediately. The limit $V_c(0) \rightarrow 0$ does not apply because then the particle would reside in the nonadiabatic regime. Initially circular orbits ($e_0 = 0$) take the longest to achieve a flat orbit but can still easily reach that orbit. Additionally, the ratio in parenthesis is proportional to the reciprocal of the mass loss adiabaticity index from Veras et al. (2011), and this index could be used to help ensure adiabaticity is maintained (so that equation A10 remains valid) as the eccentricity increases.

While stretching and contracting, the pericentre of the orbit evolves according to

$$\frac{d\omega}{dt} = \frac{3\sqrt{1-e(t)^2}}{2e(t)M_s(t)} \sqrt{\frac{a(t)}{G(M_s(t) + M_p)}} u \dot{M}. \quad (\text{A11})$$